RAPID CALCULATION OF THE BACKSHEET COUPLING GAIN USING RAY GROUPS

Andrea Pfreundt, Max Mittag
Fraunhofer Institute for Solar Energy Systems ISE
Heidenhofstraße 2, 79110 Freiburg
andrea.pfreundt@ise.fraunhofer.de

ABSTRACT: Internal reflections within photovoltaic modules are known to contribute to power gains from cell to module. The module rear cover, usually a white backsheet, is one module component reflecting additional light onto the solar cell. A novel approach to model the effect of backsheet reflectance on the achievable coupling gain in solar modules is presented. Using a discrete ray optics approach, results can be calculated rapidly for arbitrary reflectance distributions using a partition of the emerging rays into groups. The model is fully wavelength resolved, using measured data to model optical material properties. It is therefore suitable for arbitrary material stacks in front of and behind the solar cell with a single diffusely scattering layer. We study the impact of layer thicknesses, incidence angle and distribution function on the coupling gain using the presented approach. Comparison to measurements of the coupling gain using single cell modules shows good agreement with the calculated results.
Keywords: PV Modules, Ray Tracing, Simulation, Module Efficiency, Coupling Gains

1 INTRODUCTION

Cell-to-module (CTM) efficiency losses in photovoltaic modules due to inactive module areas account for up to 2.5% abs. for a common module setup with 2 mm cell and string distance. Additionally, optical losses due to parasitic absorption and reflection contribute approximately 0.8% abs. [1, 2]. Light recycling from inactive module areas such as cell spacing and the outer module border contributes as coupling gain and reduces these losses [3, 4]. The magnitude of the coupling effect depends mainly on cell spacing, optical properties of the encapsulation materials and the reflectance of the module rear side [5][6]. Several methods to enhance the effect have been demonstrated, such as light redirecting ribbons and structured backsheets [7]. Experimental methods to investigate the coupling gain rely on short circuit current measurements of module samples with apertures or defined cell spacing. Either a single sample is built for each configuration [4, 5] or different backsheets are coupled to the same module stack by a liquid coupling agent to improve comparability [8].

In this paper we are presenting a computational approach based on data from transmission and reflection measurements of the individual encapsulation materials and geometric parameters of the module stack. The model enables rapid analysis of the coupling gain for parameter variations, including layer thickness, angular dependence and consideration of bifacial cells. It is compatible to the module simulation software SmartCalc.CTM and can be used as an integral part of the module simulation.

2 Simulation Methods

2.1 Cell-to-module loss analysis

The calculation method is compatible to the CTM methodology of the cell-to-module analysis tool SmartCalc.CTM. As published earlier, optical loss factors due to reflection and absorption for the front and rear encapsulation layers are calculated from measured material data [5]. The previously used model has been extended to incorporate the dependence of each of these optical factors on the angle of incidence (AOI). The relevant loss factors are listed in Table I.

Table I: Definition of optical loss factors

Symbol	Description
$\boldsymbol{k_3}$	Air/cover reflection
$\boldsymbol{k_3^{inv}}$	Cover/air reflection
$\boldsymbol{k_4}$	Cover absorption
$\boldsymbol{k_5}$	Cover/encapsulant reflection
$\boldsymbol{k_5^{inv}}$	Encapsulant/cover reflection
$\boldsymbol{k_6}$	Encapsulant absorption

The radiant flux (or power P) on the cell front through the encapsulation layers of the module P_{ref} is calculated from these loss factors and acts as a reference for the calculation of the backsheet gain. P_0 is the incident flux onto the module surface.

$$P_{ref}(d) = P_0 \cdot k_3 \cdot k_4 \cdot k_5 \cdot k_6 \tag{1}$$

The gain associated with the reflectance of the backsheet is denoted as k_{bs}. For a given cell spacing d it is defined as follows:

$$k_{bs}(\mathrm{d}) = 1 + \frac{P_{bs}(d)}{P_{ref}} \tag{2}$$

$$\Delta \mathrm{I_{sc}}(\mathrm{d}) = \frac{I_{sc}(d)}{I_{sc,0}} \tag{3}$$

The radiant flux $P_{bs}(d)$ describes the light that is redirected onto the cell via the surrounding backsheet. Similar definitions exist using the short circuit current as the defining parameter, which can be measured directly using module prototypes. We use the short circuit current gain, defined in (3), to characterize the backsheet coupling gain. Assuming a linear relationship between irradiance and short circuit current is valid for the considered range of irradiances [9], making the two values comparable but neglecting changes in voltage. We use (2) when analyzing module prototypes as described further down. Another option to evaluate backsheet reflection gains is to define the recovery probability of the backsheet, which considers the short circuit current gain per visible backsheet area [8]. We choose the first approach as it directly relates to current gain of the

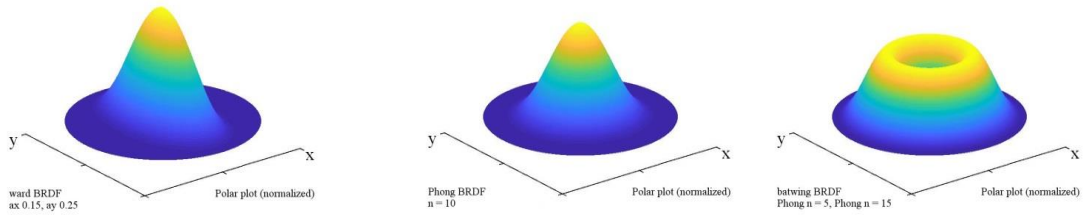

a) Ward model **b)** Phong model **c)** Phong model (batwing)

Figure 1: Different bidirectional reflectance distribution functions (BRDF) to model backsheet reflectance. All BRDFs are normalized to the same total reflectance. The ward parameters are $\alpha_x = 0.15$ and $\alpha_y = 0.25$. The Phong distribution is modeled with n = 10. The batwing model is based on two Phong distributions with n = 5 (base) and n = 15 (dip).

individual cell and makes it possible to consider cells with different surrounding geometries in one module and subsequently analyze the impact on electrical module losses.

2.2 Ray group model

2.2.1 Backsheet reflectance models

The backsheet reflectance distribution function (BRDF) is modeled by one of three approaches commonly used in ray tracing; Lambert, Phong or Ward distribution. The Lambertian reflectance model (not shown in the figure) considers a totally diffuse reflectance with a uniform distribution of the reflected light independent of the direction of the incoming/outgoing ray. The Phong model adds a specular peak (gloss lobe in rendering) to the Lambertian distribution, the width of which is determined by a parameter *n* that enters as exponent on the cosine of the angle between incident and reflected rays. The Ward distribution is capable of modelling an anisotropic distribution by adding a Gaussian specular glare with two main axes defined by their variances α_x and α_y. Examples of BRDFs based on these models are shown in Figure 1. It is possible to use other functions or measurement data to replace these models, for example to simulate structured backsheets or in order to optimize the reflectance for a specific module setup. We use hemispheric reflection data obtained from an integration sphere, which collects all the reflected light over the full hemisphere or with an additional opening of approximately 8° to exclude the direct reflection component. This results in a total hemispheric as well as a diffuse reflection spectrum. For mostly diffusely scattering backsheets we expect the direct component of the reflectance in air to disappear in the laminated module due to fusion between backsheet surface and encapsulation material.

2.2.2 Definition of ray groups

We partition the light reflected at the backsheet at each location x into ray groups. The x axis origin is located at the cell edge, pointing away from the cell. Each group is characterized by a predetermined trajectory through the encapsulation materials and a landing point on one of the areas of the solar cell (front, side, back). In this way, the pre-calculated optical loss factors of the encapsulation layers are reused to build an angle dependent loss function by matrix multiplication for each ray group. Loss function and BRDF are denoted with an M to indicate their discrete character as pre-calculated matrix in the implementation. For the zenith angle θ and azimuth angle φ the loss matrix for the cell front and back is calculated as follows:

$$M_{cf}^{k}(\theta) = [k_6(\theta)]^2 \cdot k_5^{inv}(\theta) \cdot k_4(\theta) \cdot (1 - k_3^{inv}(\theta)) \cdot k_4(\theta) \cdot k_5(\theta) \cdot k_6(\theta) \quad (4)$$

$$M_{cb}^{k}(\theta) = k_6(\theta) \quad (5)$$

The subscript indicates the location where the ray path terminates (e.g. cf = cell front). Since the encapsulation materials are assumed to be isotropic, M is independent of the azimuth angle φ.

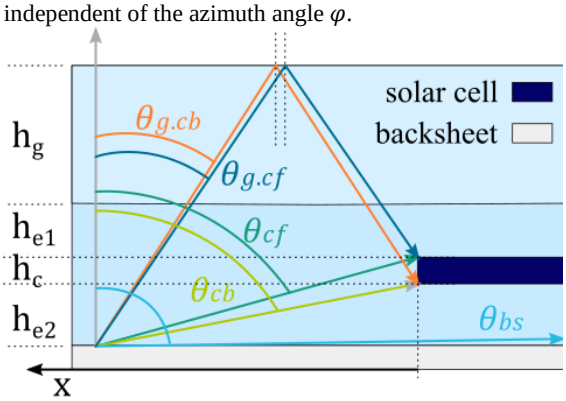

Figure 2: Illustration of the zenith threshold angles that divide the ray groups into sections on the reflected half sphere. For each azimuth angle φ and distance *x* from the cell edge these angles can be calculated directly from the geometry of the module.

The geometry of the module is modeled by defined layer thicknesses and a given cell spacing. For each distance from the cell edge, threshold angles can be defined that bound the ray groups and enable the calculation of their contribution without explicitly calculating each ray trajectory and interface intersection. The threshold angles are illustrated in Figure 2. The extent of the cell is not shown but considered in the calculation of the ray groups reaching the cell front and backside.

Calculation of the threshold angles is straightforward from geometrical considerations:

$$\varphi_0(x) = \tan^{-1}\frac{w_{cell}}{x} > 82°, \text{for relevant x} \quad (6)$$

$$\theta_{g.cf}(\varphi, x) = \tan^{-1}\frac{x/\cos\varphi}{2h_g + 2h_{e1} + h_{e2}} \quad (7)$$

$$\theta_{g.cb}(\varphi, x) = \tan^{-1}\frac{x/\cos\varphi}{2h_g + 2h_{e1} + h_{e2} + \frac{1}{2}h_c} \quad (8)$$

$$\theta_{cf}(\varphi,x) = \tan^{-1}\frac{x/\cos\varphi}{h_{e2}+\frac{1}{2}h_c} \quad (9)$$

$$\theta_{cb}(\varphi,x) = \tan^{-1}\frac{x/\cos\varphi}{h_{e2}} \quad (10)$$

$$\theta_{bs}(\varphi,x) = \tan^{-1}\frac{w_{cell}+x}{h_e\cos\varphi} \approx \frac{\pi}{2} \quad (11)$$

Table II: Definition of ray groups by reflectance angle

Index	Description	Condition for θ
g.bs	Backsheet via glass reflection	$\theta \le \theta_{g.cb}$
g.cs	Cell side via glass reflection	$\theta_{g.cb} \le \theta \le \theta_{g.cf}$
g.cf	Cell front via glass reflection	$\theta_{g.cf} \le \theta \le \theta_{cf}$
cs	Cell side directly	$\theta_{cf} \le \theta \le \theta_{cb}$
cb	Cell back directly	$\theta_{cb} \le \theta \le \theta_{bs}$

Since each side of the solar cell is a continuous surface, only one ray group needs to be considered from each point on the backsheet, leading to the definition of 5 ray groups not considering multiple reflections which are shown in Table II. The irradiance originating from a point at distance *x* from the cell edge is defined as

$$\mathrm{E}_{group}(x) = \mathrm{E}_{bs}(x)\cdot f_{bs.cf}(d) \quad (12)$$

$$f_{bs.\mathrm{cf}}(d) = \frac{\int_{-\varphi_0(x)}^{\varphi_0(x)} d\varphi \int_{\theta_1(\varphi,x)}^{\theta_2(\varphi,x)} d\theta \ \sin\theta \ M_{BRDF}(\theta,\varphi)M_{cf}^{k}(\theta)}{\int_{-\pi}^{\pi} d\varphi \int_{0}^{\pi} d\theta \ \sin\theta \ M_{BRDF}(\theta,\varphi)} \quad (13)$$

The angle φ_0 is defined by the lateral extent of the cell along the cell edge. An average value of half the cell length is assumed. $\theta_1(\varphi,x)$ and $\theta_2(\varphi,x)$ are defined by the module geometry in *x* direction and layer thicknesses; they are unique for each of the ray groups (see Table II).

The total radiant flux (or power *P*) incident on the cell is determined by integration over all contributions in the given ray groups from the backsheet area corresponding to a specific cell distance.

$$\begin{aligned}\mathrm{P}_{group}(d) &= dA\ \mathrm{E}_{group}(d)\\ &= dy\int_0^d dx\ \mathrm{E}_{group}(x)\\ &= dy\ P_{group}^{y}(d)\end{aligned} \quad (14)$$

2.2.3 Multiple reflections

For one setup of the model with a maximal cell distance all smaller cell distances are calculated simultaneously. Light that is scattered in backward direction (away from the cell) can contribute to the backsheet gain by way of multiple reflection. While the consideration of this additional reflection in detail would increase model complexity, the maximal contribution for each cell distance *d* is readily obtained in the simulation (group 1) and can be used to estimate the total contribution of multiple reflections. An average of the ray groups reaching the cell is used to scale the redirected light and calculate the additional contribution to the total power on each cell area. Exemplary for the cell front

$$\mathrm{P}_{g.bs.cf}(d) = \mathrm{P}_{g.bs}(d)\cdot\frac{f_{bs.cf}(d)}{d} \quad (15)$$

where integral in (13) is scaled with the total area to average the contributions over the full length. This is a simplification that neglects the landing point of multiply reflected rays on the backsheet.

2.2.4 Shading at non-normal incidence

Variation of the incidence angle leads to a reduction in incident light and shading of the cell within the cell spacing. This is considered in the model by shifting the integration boundaries of the integral in (14). The contributions from the four sides of the cell are accounted for individually (for varying azimuthal angles). As illustrated in Figure 3. For a change in zenith angle, x_{s1} and x_{s2} are added to/subtracted from the integration boundaries when integrating the contributions from the cell spacing area. Considering variations in azimuth angle requires the calculation of shading distances on all 4 sides of the cell.

$$x_{s,1}(\theta_{t2},\varphi) = h_{EVA}\tan\theta\sin\varphi \quad (16)$$

$$x_{s,2}(\theta_{t2},\varphi) = (h_{EVA}+h_{cell})\tan\theta\sin\varphi \quad (17)$$

$$y_{s,1}(\theta_{t2},\varphi) = h_{EVA}\tan\theta\cos\varphi \quad (18)$$

$$y_{s,2}(\theta_{t2},\varphi) = (h_{EVA}+h_{cell})\tan\theta\cos\varphi \quad (19)$$

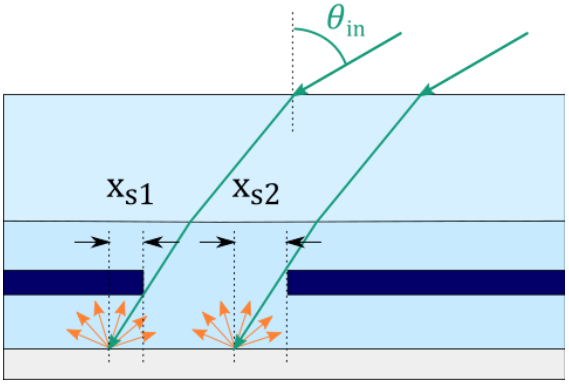

Figure 3: Shading of the visible backsheet area due to variations in the angle of incidence leads to additionally illuminated area at x_{s1} and shaded area x_{s2}.

2.2.5 Implementation of the ray group model

The model has been implemented in MATLAB and made compatible with the simulation software SmartCalc.CTM. The result of the optical simulation of the module layers, which is based on measurement data, is used as input to the ray group calculation. This makes it possible to incorporate the calculation method for backsheet coupling gains into the full cell to module loss calculation.

3 EXPERIMENTAL METHODS

3.1 Short circuit current measurements

Mini-modules consisting of a single solar cell embedded in the module stack are fabricated with different white and black backsheets. The hemispheric and diffuse reflectance of the backsheets is obtained using an integrating sphere, the direct contribution is

calculated as the difference of the two measurements and corresponds to the reflected light into an opening angle of approximately 8° from the surface normal.

The open circuit current is measured at STC conditions using a Xenon Lamp calibrated to 1000 W/m². Aperture masks are used to limit the incident light to an area around the cell corresponding to different cell spacing in order to measure the contribution of this area to the individual cell current. A mask with a 135 mm opening is used in addition to the 156 mm mask as control to limit the influence of stray light. We estimate the error of cell distance due to placement of the mask and the influence of stray light to be around 0.25 mm. Examples of the used masks are shown in Figure 8 and the setup is illustrated in

Figure **9**.

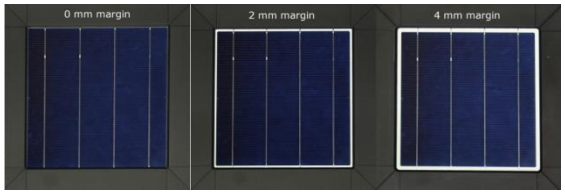

Figure 8: Layout of the apertures (masks) to measure the coupling gain for a specific margin where the backsheet is visible. The margin corresponds to the full cell distance in the simulations.

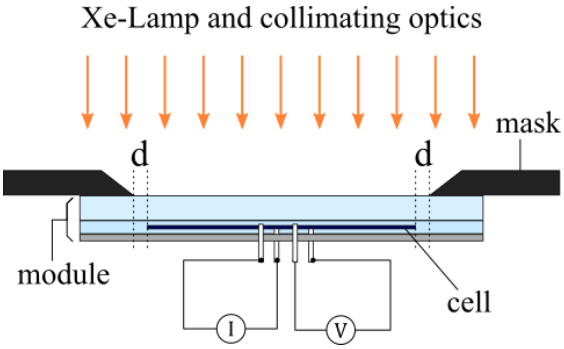

Figure 9: Schematic illustration of the measurement setup to measure the short circuit gain associated with backsheet coupling effects. A sun simulator with a total flash intensity of 1000 W/m² in the module plane is used for illumination.

4 RESULTS

4.1 Contributions of different areas on the cell to the backsheet coupling gain

By using ray groups it is straight forward to analyze the contribution of different cell areas to the backsheet

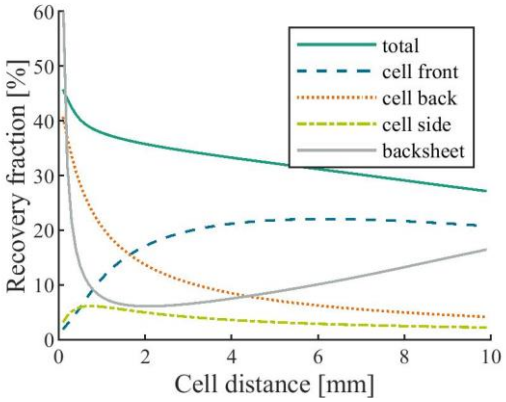

Figure 4: Contribution of the different cell areas to the backsheet coupling gain expressed as total recovery fraction of the light incident on the cell gap for each cell distance.

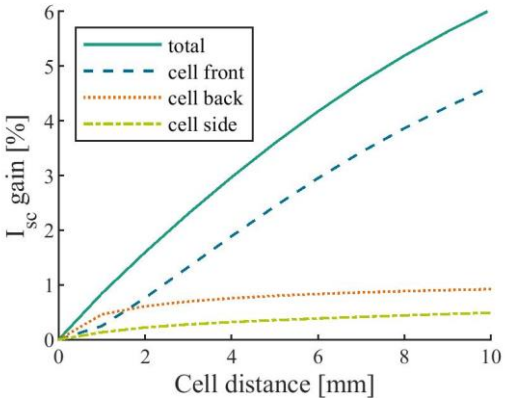

Figure 5: Calculated contribution of the different cell areas to the backsheet coupling gain expressed relative short circuit current gain of an individual cell surrounded by a cell gap of the specified size (cell distance).

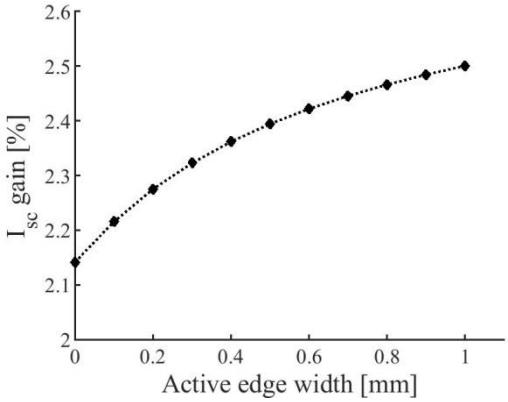

Figure 6: Backsheet coupling gain for a cell distance of 4 mm and different widths of the active area on the cell backside.

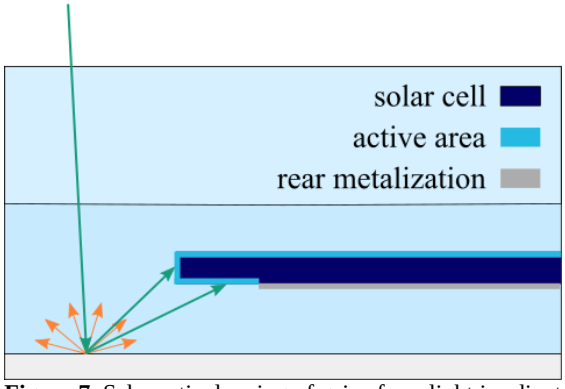

Figure 7: Schematic drawing of gains from light irradiant on the solar cell rear and side after backsheet reflection.

coupling gain. The collected contributions for each cell area are shown in Figure 5 for a typical solar module setup using bifacial solar cells and a totally diffuse reflecting backsheet with a reflectance of 82%, modeled using Lambertian reflection. The fraction that returns to the backsheet via the glass surface is also shown. This contribution as well as the contribution on the cell back side start at very high recovery values, since the impact of the lateral extent of the cell gap contributes significantly. Since the absolute irradiance entering the cell gap for small gap sizes is small, the absolute contributions will be small, as seen in the following results, which are shown in terms of as absolute current gain for an individual cell.

Today most industrial cells are "monofacial" which is a term used to describe that the rear side is usually blocking incident light and therefore light from the rear is not contributing to power generation. We find the assumption of complete photoelectrical inactivity of the solar cell rear side to be insufficient to describe effects of backsheet gain. Common cells feature a margin between the cell edge and blocking rear side cell metallization (i.e. aluminum) which leads to active cell areas on the cell rear side. Since these areas are located near the cell edge additional backsheet gains can be realized (Figure 7).

Measurements at Fraunhofer ISE CalLab Cells of the generated photocurrent at the edge and backside of monofacial cells have shown current density levels of 70% and 85% respectively compared to the front side. This significantly adds to the gain that can be obtained through backsheet coupling. Simulations show an increase from 2.15 % to 2.4 % for a cell distance of 4 mm and an active backside edge of 0.5 mm.

Figure **6** shows the simulation result for a variation of the backside contribution for a fixed cell distance of 4 mm.

4.2 Impact of incidence angles on the relative backsheet coupling gain.

Variation of the zenith incidence angle between 0° and 80° has a very small impact on the backsheet gain. For cell distances up to 10 mm, the effect is less than 0.07 % across all angles. Variations in the azimuthal angle have no impact on the coupling gain as long as the reflection of the backsheet is isotropic. The different shading effects on the four cell edges cancel each other for a rectangular cell. The cell thickness has a small impact on the discrepancy between the shading distances of the opposite cell sides (Figure 3 and (16)-(19)), but the effect is found to be negligible in the studied cases.

4.3 Variation of geometrical parameters

4.3.1 Glass thickness

The thickness of the glass cover affects the coupling gain due to higher absorption of the reflected rays reaching the cell front, which shows especially at longer distances from the cell edge. The results in Figure 10 show that for thicker glasses the dependence of the coupling gain on cell distance changes from an exponential behavior towards a linear curve for distances up to 10 mm. For thicker glasses the exponential behavior is shifted to higher distances. Since the module standard for glass thicknesses moves towards thinner glasses, it is not sufficient to assume a linear model and it is necessary take the geometry into consideration.

4.3.2 Encapsulation thickness

The encapsulation thickness influences the coupling gain due to additional absorption in the polymer and by changing the light distribution in the ray groups due to the changes in geometry. For common EVA films we find a significant variation in coupling gain between 0.5 % and 1.2 % for common cell distances and for a range of EVA thickness between 150 µm and 900 µm corresponding to half respectively double the most common encapsulation sheet thickness. Figure 11 shows the variation with cell distance which is largest for common cell distances between 2 mm and 6 mm. Small variations in the encapsulation thickness which might arise due to differences in the lamination process will not have a significant influence on the backsheet coupling gain as we see in the curves in Figure 12, but will lead to uncertainties of approximately 0.1% per 100µm when values are compared with measurements.

4.3.3 Cell thickness

The influence of the cell thickness is investigated for common solar cells between 100 µm and 250 µm. Simulations show a variation of the coupling gain due to the increased surface area of the cell sides below 0.1 % for cell distances up to 10 mm. Compared to the impact of other parameters, this is a negligible contribution.

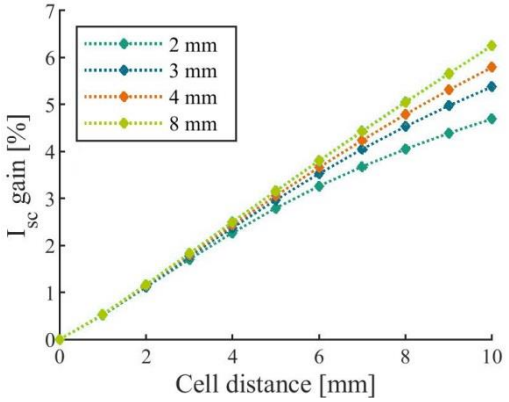

Figure 10: Backsheet coupling gain for identical module stacks with different glass thicknesses.

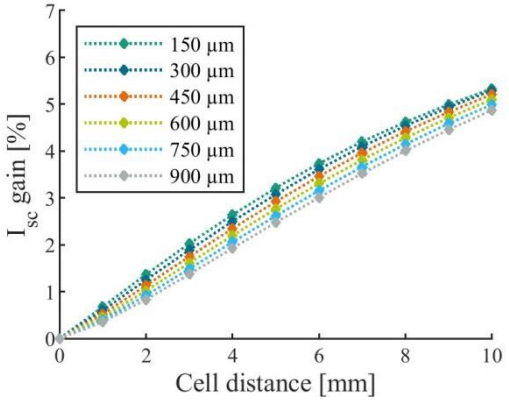

Figure 11: Backsheet coupling gain for different encapsulation thicknesses and cell distances. The thickness is the same on front and rear side of the cell.

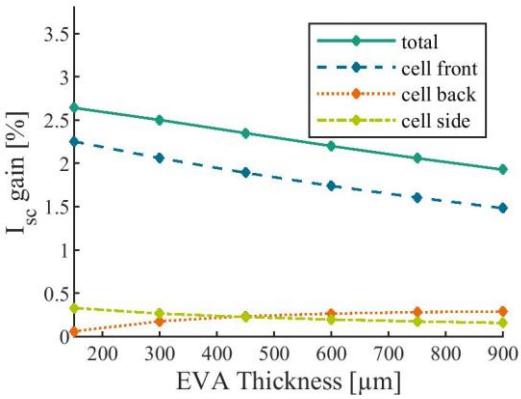

Figure 12: Backsheet coupling gain for a cell distance of 4 mm split into contributions from the different areas of the cell (ray groups) for a variation of the encapsulation thickness between 150 µm and 900 µm.

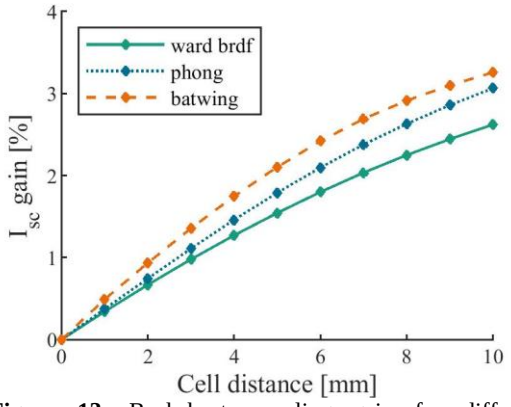

Figure 13: Backsheet coupling gain for different reflection distributions shown in Figure 9. For a total BRDF distributed reflectance of 75 % and 25 % diffusely distributed.

4.4 Comparison of BRDFs

Different bidirectional reflectance distribution functions (BRDFs) can be used to describe backsheet reflection. Ideally, precise measurements are performed to determine the distribution function. As these measurements are quite expensive and time consuming it is advisable to model the distribution function based on a few measurement parameters. Commonly the Lambertian distribution is used to model perfectly diffusive reflection behavior.

The shape of the reflection function influences the light distribution among the ray groups. Figure 1 shows three different light distributions, modeled with different approaches. a) shows an isotropic Phong distribution with n = 10, b) shows a non-isotropic Ward distribution with FWHMs of 0.15 and 0.25 in x (perpendicular) and y (parallel to cell edge) directions respectively, c) shows a batwing distribution. All BRDFs are normalized to the same total reflectance. The resulting coupling gain for different cell distances is shown in Figure 13.

4.5 Comparison of ray group calculation results with measurement data

The short circuit current gains associated with backsheet coupling are measured on single cell modules with different backsheets. The modules are built with monofacial solar cells, 450 µm EVA sheets and 3 mm solar glass without anti-reflective coating. For the simulation the reflection and transmission spectra of the individual materials are used to model their behavior. The cell surface and influence of metallization on the front side is not considered. The shape of the resulting curves shows an excellent agreement with the measured data while the absolute values show minor discrepancies (Figure 14). The individual contributions of the three cell areas are shown. We assume an active cell edge on the backside of 450 µm in the simulation, which is responsible for the contribution of the cell backside. A measurement tolerance in the effectively visible backsheet area due to stray light that enters the apertures at an angle is estimated to be of the order of 0.25 mm. Considering that this might lead to a shift in the measured data, we conclude that the presented model can be used to calculate the backsheet coupling gain with good accuracy.

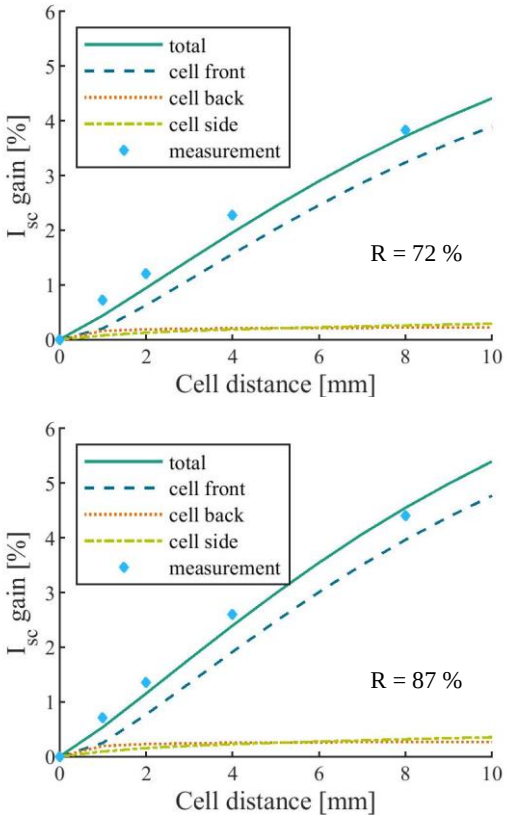

Figure 14: Measurement and simulation of backsheet coupling gain. The simulated gain is shown for different ray groups as well as the total gain. The measurement data is shown as diamonds. Data is shown for two backsheets with a reflectance of 72 % and 87 %.

5 SUMMARY AND OUTLOOK

We present an approach to rapidly calculate the backsheet coupling gain for individual cells in solar modules by using a model based on ray groups. The method is a simplified discrete ray optics approach, based on the explicit calculation of all the emerging rays. By dividing the reflected rays emerging from a diffusely scattering surface into ray groups by threshold angles, no ray tracing is necessary. This reduces the required number of calculations significantly. We show the simulation of backsheet coupling gains for a range of

parameter variations such as geometrical parameters and reflection behavior of the backsheet. The presented method enables us to investigate new module setups with arbitrary backsheet reflectance functions in terms of achievable current gains. It simplifies the investigation of structured surfaces with complex reflection behavior, which can now be modeled to study their impact on module performance. Since the incidence angle in the module plane can be varied, the impact of the coupling gain on the yearly solar energy yield can be included in performance analyses.

We analyze the backsheet gain in terms of contributions from different reflection paths and find the reflection via the front cover to be the most important. We confirm a significant contribution of the cell side and rear, which is predominant for small cell distances. Our analysis of different module setups shows glass thickness to increase the backsheet coupling gain at long cell distances which is relevant for the effect on module margins. The thickness of encapsulants has a minor impact, while the effect of cell thickness is negligible. We investigate the dependence of incidence angle on the backsheet coupling gain and find that due to the symmetrical setup, shading effects balance resulting in virtually no dependence of the relative coupling gain on incidence angle. For non-isotroptic scattering backsheets such as structured surfaces we expect a stronger dependence on the angle of incidence that can have implication for annual yield analysis. Our present results confirm the importance of backsheet coupling for cell to module loss analysis. The method enables the quantification of the associated gains and their consideration for module optimization and evaluation of trade-offs between total module area and inactive area gains.

6 ACKNOWLEDGEMENT

We would like to thank the German Federal Ministry of Economic Affairs and Energy (FKZ 0324033) for their funding.

7 REFERENCES

[1] M. Mittag *et al.*, "Systematic PV module optimization with the cell-to-module (CTM) analysis software," *Photovoltaics International*, no. 36, pp. 97–104, 2017.

[2] *cell-to-module.com.* [Online] Available: http://www.cell-to-module.com. Accessed on: Feb. 28 2018.

[3] O. Dupré *et al.*, "Reassessment of cell to module gains and losses: Accounting for the current boost specific to cells located on the edges," in *Silicon PV 2018*, p. 90001.

[4] M. Mittag *et al.*, "Analysis of backsheet and rear cover reflection gains for bifacial solar cells," *33rd European PV Solar Energy Conference and Exhibition*, vol. 2017.

[5] I. Hädrich *et al.*, "Unified methodology for determining CTM ratios: Systematic prediction of module power," *Solar Energy Materials and Solar Cells*, vol. 131, pp. 14–23, 2014.

[6] P. Grunow *et al.*, "Modelling of the Encapsulation Factors for Photovoltaic Modules," 4th IEEE WCPEC, Waikoloa, Hawaii, USA, 2006, pp. 2152–2155.

[7] M. R. Vogt *et al.*, "PV module current gains due to structured backsheets," *Energy Procedia*, vol. 124, pp. 495–503, 2017.

[8] M. Köntges *et al.*, "Method to measure light recovery probability of PV module backsheets enabling 20.2% module efficiency with passivated rear emitter and rear solar cells," *32nd Eurpean Photovoltaic Solar Energy Conference (EUPVSEC)*, vol. 2016, 1532–1538.

[9] A. Schmid *et al.*, "IV Measurement of Bifacial Modules: Bifacial vs. Monofacial Illumination," 33rd EUPVSEC, Amsterdam, 2017, pp. 1624–1627.